Proceedings of the ASME 2010 3rd Joint US-European Fluids Engineering Summer Meeting and 8th International Conference on Nanochannels, Microchannels, and Minichannels
FEDSM-ICNMM2010
August 1-5, 2010, Montreal, Canada

FEDSM-ICNMM2010-30751

ROTATING MICROSENSORS WITH NON-LINEAR FEEDBACK

Andrew R. Sloboda
Department of Mechanical Engineering
University of Michigan
Ann Arbor, Michigan 48109
Email: asloboda@umich.edu

Bogdan I. Epureanu*
Department of Mechanical Engineering
University of Michigan
Ann Arbor, Michigan 48109
Email: epureanu@umich.edu

ABSTRACT

The need for instruments that detect and quantify small amounts of chemical and biological agents has spurred the development of micro-scale and nano-scale resonators. Most of these sensors are variations of vibrating cantilever beams and rely on resonant frequency shifts to quantify added mass. While very sensitive in vacuum or low viscosity environments, these types of sensors suffer performance degradation in viscous fluids, where damping is significantly increased.

This paper presents a unique sensor architecture consisting of an immersed micro-plate designed to vibrate rotationally about an axis as fluid flows past it in a micro-channel. The idea behind this design is that some of the energy in the incoming flow can be harvested due to fluid-structure interaction, thereby reducing the effective damping. Only a small outside energy input is then required to obtain sustained, large amplitude vibrations.

We show how sensitivity vector techniques applied to such a device can provide an alternate means of effectively detecting small mass variations. A method of optimizing the feedback control in order to maximize sensitivity using a spline-based force surface spanning the state space is also presented.

INTRODUCTION

Detecting and characterizing small amounts of chemical and biological agents is important in many health and defense related applications. Fast and reliable identification of trace amounts of materials can be crucial for correct assessment and response in scenarios ranging from diagnosis of bacterial infections to counter-terrorism screening.

One way of providing chemical and biological detection is through the use of active, vibration-based micro-sensors. Typical vibration-based sensing methods apply a system excitation to the sensor and then monitor the dynamic response, which changes when the substance of interest is present. Frequency-shift methods based on changes in resonant frequencies caused by particles binding to a vibrating microstructure are examples of this approach [1, 2]. Unfortunately, when sensors exhibit nonlinearity, significant damping, or when sensor properties are liable to change over time (due to, for example, environmental changes or sensor damage), these frequency-shift based methods can lead to unsatisfactory results.

The case of vibration-based sensing in highly damped environments is of particular interest because detecting and quantifying particles in liquids is often necessary. For instance, being able to quantify different types of particles in a lab-on-a-chip environment could improve medical diagnosis. Resonant-frequency based detection is often poor in such damped environments because the quality factor is diminished and the resonant peak is no longer sharp. Burg and collaborators [3] constructed a resonator where flow is channeled within the resonating structure itself as one possible solution to this problem.

An alternate approach, taken here, is to minimize the effective damping by designing an immersed sensor which takes advantage of the flow to recover some of the energy lost to damping. This is challenging because only low Reynolds number flows are practical in liquid MEMS [4, 5]. Work on rotational

*Address all correspondence to this author.

galloping of prismatic structures is of particular interest, as we would like our system to be as near to this type of behavior as possible [6,7].

In order to measure changes in system properties, such as added mass, we make use of an alternate metric known as sensitivity vector fields (SVFs) which quantify how attractors deform [8,9]. SVFs are constructed by sampling system trajectories that diverge due to parametric variations and using the resulting snapshots of the deformation as references when the system changes under operating conditions. The SVF approach has several advantages. In many cases, using SVF analysis means that nonlinear features of the system can be enhanced and exploited to increase sensitivity rather than hindering the interrogation. As well, simultaneous sensing of multiple analyte properties with a single sensor is sometimes possible since we are dealing with vector, rather than scalar, features/quantities. Originally developed for structural health monitoring [10–12] in mechanical systems, SVF techniques have since been used to detect parameter variations in a variety of dynamical systems, including tapping mode atomic force microscopes [13].

The key to effectively utilizing SVF techniques is the design of nonlinear feedback controllers. These controllers need to provide system excitation which maximizes attractor deformations caused by changes in parameters of interest (thereby enhancing sensitivity) while minimizing attractor deformations caused by changes in other system parameters (thereby improving selectivity). We demonstrate how to design such controllers for a sensor using spline surfaces of feedback force optimized to enhance sensitivity.

NOMENCLATURE

$\mathbf{A}$	nominal trajectory Jacobian
A	harmonic excitation magnitude
$\mathbf{B}$	nominal trajectory parameter derivative
E	silicon elastic modulus
G	silicon shear modulus
H	channel height
I	section moment of inertia
W	channel width
b	damping parameter
k	torsional spring stiffness
p	perturbed parameter
p_o	nominal value of perturbed parameter
δp	variation in perturbed parameter
$\mathbf{q}$	normalized sensitivity vector
x	position
$\dot{x}$	velocity
x_n	state component n
$\mathbf{x}$	state vector
$\delta\mathbf{x}$	variation in state vector
ΔT	trajectory evolution time
Φ	state transition matrix
α	plate angle
θ	angular displacement
ρ	fluid density
ρ_s	silicon density
ω	harmonic excitation frequency
ω_n	natural frequency
ζ	damping coefficient

SENSOR DESIGN STRATEGY

The primary challenge in designing an effective vibration-based micro-sensor for a liquid environment is overcoming, as much as possible, the high level of damping due to the viscosity of the liquid. Unlike in a near-vacuum or gas environment where damping can often be neglected, in liquids damping effects are not negligible and make frequency-shift based measurement difficult. In order to combat damping, the sensor must be designed in such a way that the effects of damping are reduced or measurements must be made using an alternate method that is more sensitive to the desired analyte. Here we explore both of these options.

One strategy to try and overcome the high level of damping in a liquid is to harvest some energy from the oncoming flow to make up for the energy lost to damping. Examples of this type of energy gain include vibration-based energy harvesters [14,15]. In some of these systems, the energy harvested from the flow reduces the effective damping experienced by the harvester until it is negative, and sustained motion ensues.

It is unclear if this type of energy harvesting is possible in an enclosed channel on the micro-scale. Simulations of rotational galloping found in the literature do not deal with high blockage ratios [6]. Additionally, inertial forces are small relative to viscous forces, and thus flows are restricted to low Reynolds numbers. If we consider a sensor in a square cross-section channel with dimensions on the order of tens of micrometers, we can expect pressure losses to be calculated similarly to a macro-scale system [4]. Using relevant micropump data [5] we can estimate the range of practical Reynolds numbers and pressure losses for channels of different cross-sections and lengths. For example, Figure 1 shows a plot of uniform velocity and pressure drop over a 1mm length channel for a micropump with a maximum flow rate of 4.4 mL/min [5]. The acceptable pressure drop in this case is 21 kPa so we would consider cross-sections larger than 100 um by 100 um. For these sorts of dimensions, Reynolds numbers based on a 10 um face dimension will only be on the order of hundreds.

FLUID SYSTEM SIMULATIONS

To investigate the potential for energy harvesting, we consider two different sensor geometries. The first geometry consists

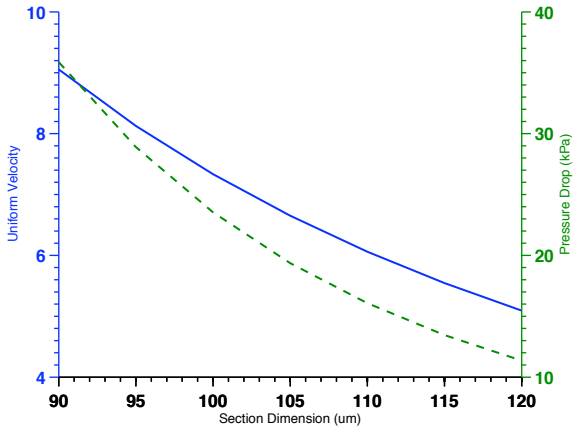

FIGURE 1. UNIFORM VELOCITY AND PRESSURE DROP FOR A 1 mm CHANNEL

of a flat plate that pivots about its geometric center with its pivot centered in the channel flow. Its largest face is parallel to the upper and lower channel walls when there is no flow as shown in profile in Figure 2. The channel considered is this case has $H = 100$ um and $W = 100$ um. The other relevant dimensions are $D = 10$ um and $L = 40$ um. The second geometry is also a flat plate, but its largest face is nominally at an angle of α to the upper and lower walls. Its pivot point is offset far from the geometric center of the plate and is also away from the center of the channel as shown in profile in Figure 3. The channel considered has $H = 75$ um and $W = 150$ um. Here $D = 10$ um, $L = 90$ um, and the angle α is 12°. The surrounding channels are 600 um long. These geometries were selected as test cases because they are known to produce galloping-type instabilities under certain flow conditions [16].

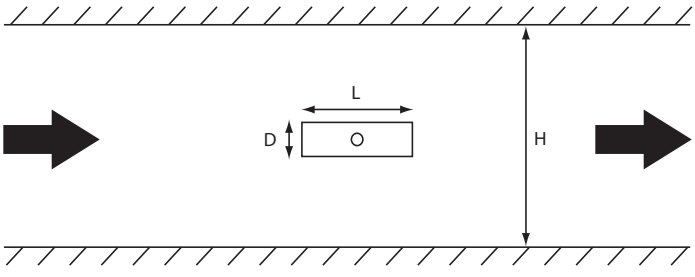

FIGURE 2. FIRST SYSTEM FLOW GEOMETRY

The plates were considered to be made of silicon with nominal properties of $E = 150$ GPa, $G = 64$ GPa, and $\rho_s = 2330\,\mathrm{kg/m^3}$. The liquid was treated as water with $\rho = 998.2\,\mathrm{kg/m^3}$. The geometries of these sensors were generated

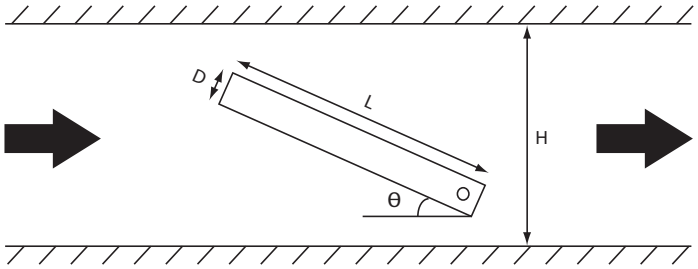

FIGURE 3. SECOND SYSTEM FLOW GEOMETRY

in two forms for simulation in ANSYS CFX. One version was essentially two dimensional, consisting of a mesh a single element thick, while the other contained the full system geometry, including the plates meshed as solid bodies, and took advantage of the symmetry at the channel midline. These systems were primarily meshed with tetrahedral elements. A close-up view of the mesh around one of the bodies is shown in Figure 4.

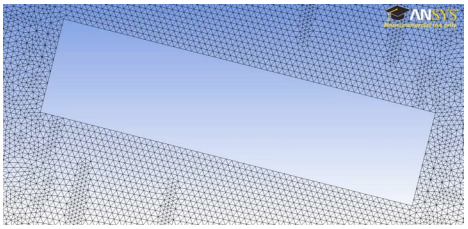

FIGURE 4. COMPUTATIONAL DOMAIN FOR SIMULATION

Initial solutions of this FSI problem were carried out by examining the system in a quasi-static manner, evaluating the moments the fluid flow applied to the cross-sections at various angles from their nominal positions. Later, using the built in solid-fluid coupling in CFX, the models were simulated transiently with various inlet flow velocities in order to ascertain the effect of increased flow speed on the effective damping. The simulation was allowed to establish a steady-state condition, and then the section was perturbed by an applied moment to a position between 5° and 10° away from the nominal position. Some time later the moment was then removed. The recorded time series of the angular displacement θ (shown in Figure 3) for such cycles was then used to determine approximate values of the damping and the damped-vibration frequency of the system, using either fractional overshoot or logarithmic decrement techniques. Figure 5 shows a times series taken just after a moment has been applied to the cross-section, demonstrating its underdamped nature. Notice the decay envelope is not perfectly symmetric due to the fluid forces involved.

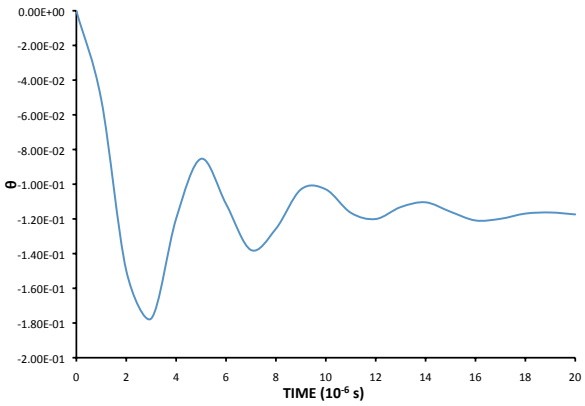

FIGURE 5. SYSTEM RESPONSE AFTER A MOMENT PERTURBATION

The transient analyses conducted using our 3D models showed displacements that are quickly damped in our two systems, with nominal damping coefficients ζ of approximately 0.2 and 0.18, respectively. As the flow rate is increased from zero flow rate to a large (and likely unrealistic value) of 5 m/s, the reduction in these damping coefficients is only about 10%.

PARAMETER EXTRACTION

Whether the damping can truly be reduced via careful sensor design in order to take advantage of the oncoming flow, the second part of our strategy remains the same: measuring sensor changes using an alternate method, not based on frequency-shifts, that is more sensitive. In order to explore this further, the fluid-structure models previously discussed are recast as one degree of freedom (DOF) systems by making use of the damping properties calculated from simulations. With damping coefficient determined, each sensor can be modeled approximately as

$$\ddot{x} + b\dot{x} + {\omega_n}^2 x = N(x,\dot{x},t) \ , \tag{1}$$

$$\text{where} \qquad \omega_n = \sqrt{\frac{k}{I}} \ , \tag{2}$$

$$\text{and} \qquad b = 2\zeta\omega_n \ . \tag{3}$$

The natural frequency is calculated by summing the moment of inertia of the section I and some 'added mass' based on the entrained fluid. Details on 'added mass' can be found in many hydrodynamics references [18]. $N(x,\dot{x},t)$ represents the overall non-linear feedback force used to excite the system. By considering states of the form

$$\mathbf{x} = \begin{bmatrix} x_1 \\ x_2 \end{bmatrix} = \begin{bmatrix} x \\ \dot{x}/\omega \end{bmatrix} \ , \tag{4}$$

this system can be converted to a standard state space form $\dot{\mathbf{x}} = \mathbf{f}(\mathbf{x},t)$ in order to apply SVF methods.

SVF THEORY

SVFs are a way to quantify attractor deformations. If two different systems with initially coincident state space trajectories are compared, one system having a nominal set of parameters and the other having some parametric variations, the trajectories of these two systems will diverge over time. By sampling the diverged trajectories a specified period of time ΔT after coincidence, a vector can be generated connecting the sampled point on the nominal trajectory with the sampled point on the varied trajectory. This is a sensitivity vector (SV). An SVF is a collection of SVs computed over a system attractor for some parameter variation. This field characterizes how the varied attractor deforms with respect to the nominal attractor.

This can be formalized mathematically by considering a state space flow described by $\dot{\mathbf{x}} = \mathbf{f}(\mathbf{x},p,t)$ where $\mathbf{x}$ is the state vector and p is the sensor readout, i.e. the parameter of interest that can be perturbed. Using a Taylor series to expand this flow about the nominal trajectory $\mathbf{x}(t) = \mathbf{x_o}(t)$ and a nominal parameter p_o one obtains

$$\delta\dot{\mathbf{x}} = \mathbf{A}(t)\delta\mathbf{x} + \mathbf{B}(t)\delta p \ , \tag{5}$$

$$\text{where} \qquad \mathbf{A}(t) = \left.\frac{\delta\mathbf{f}}{\delta\mathbf{x}}\right|_{\substack{\mathbf{x}=\mathbf{x_o} \\ p=p_o}} \ , \tag{6}$$

$$\text{and} \qquad \mathbf{B}(t) = \left.\frac{\delta\mathbf{f}}{\delta p}\right|_{\substack{\mathbf{x}=\mathbf{x_o} \\ p=p_o}} \ , \tag{7}$$

where only the linear terms are retained. Here $\delta\mathbf{x}$ is the state variation from the nominal trajectory, and δp is the parameter variation from the nominal parameter. Eq. (5) is valid as long as the discarded higher order terms remain small compared to the first order terms. For linear systems, this is always true since Eq. (5) is exact, and has no higher order terms. However, for nonlinear

systems, both the parameter variation and the state variation must remain much less than one for Eq. (5) to hold. Thus, for nonlinear systems with specified initial variations there is a limit on the evolution time for which Eq. (5) is appropriate. Integrating Eq. (5) over the evolution time results in the equivalent map

$$\delta\mathbf{x}(t_o+\Delta T)=\Phi(t_o+\Delta T,t_o)\delta\mathbf{x}(t_o)+\mathbf{q}\delta p, \tag{8}$$

where Φ, the state transition matrix for the dynamical system (sensor), depends only on $\mathbf{A}(t)$, while $\mathbf{q}$ depends on both $\mathbf{A}(t)$ and $\mathbf{B}(t)$. For two trajectories which are truly initially coincident, $\delta\mathbf{x}(t_o)=\mathbf{0}$. Thus, any separation of the trajectories that develops over the evolution time is equal to the sensitivity vector $\mathbf{q}\delta p$. As long as the evolution time is short (in order to ensure the resulting changes to system behavior are locally linear with respect to the parameter variations) the sensitivity vectors will be linearly dependent on the parameter variation. Consequently, a change in a given system parameter will elicit a proportional change in the measured attractor deformation. When examining attractor deformations, this proportionality serves as the basis for quantifying parameter changes. Often, we refer to the normalized sensitivity vector $\mathbf{q}$, which is the sensitivity vector divided by the parameter variation. As normalized sensitivity vectors are independent of the level of parameter variation, they can be helpful in comparing results.

FEEDBACK DESIGN

The next question is how to maximize a system's SVs. Obviously, the nature of the dynamical system and the choices involved in how sensitivity vectors are sampled, including things such as the evolution time ΔT, will impact the overall sensitivity. However, by changing the system through feedback, it is also possible to augment or amplify a system's natural sensitivity. Choosing an appropriate $N(x,\dot{x},t)$ in Eq. (1) has the effect of changing the system and thereby the sensitivity.

$N(x,\dot{x},t)$ will typically be subject to some constraints in a real physical system. Examples of such constraints are limits on the range of motion or velocity or the amount of force the controller can output. In this work, we also consider a limit on attractor size and penalize attractors that are too big, or too small, since SV magnitude is closely related to attractor size. Within such constraints, we can ask the question: what is the best form of feedback to maximize a specfic SVF?

Previous work by the authors [19] helped to establish some basis for answering this question by considering an $N(x,\dot{x},t)$ of the form

$$N(x,\dot{x},t)=b_c\dot{x}-k_cx-\alpha_cx^3+A\sin\omega t\ . \tag{9}$$

With $N(x,\dot{x},t)$ specified, Eqs. (1) and (5) can be integrated simultaneously to find SVs. Using this method, we were able to show the advantages and disadvantages of chaotic and non-chaotic regimes for generating SVFs with respect to parameter ω_n for different evolution times ΔT and phases of the harmonic excitation. We were also able to optimize the control parameters in the fixed controller form given by Eq. (9).

However, having a controller of fixed form, especially one with a relatively low number of polynomial terms, greatly reduces the possible distributions of feedback force across the state space. For this reason, we examine feedback that is based on control points distributed over the state space which can be interpolated with splines to arrive at an overall feedback law. This arrangement allows for a feedback force distribution that can take on a different variety of surface shapes than one based on polynomials alone. We specifically consider the case where

$$N(x,\dot{x},t)=R(x,\dot{x})+A\sin\omega t \tag{10}$$

and $R(x,\dot{x})$ is given by a spline surface of forces distributed over the state space.

The form of $R(x,\dot{x})$ can be optimized by adjusting the force values at certain control points. The positioning and number of control points may also play an important role. For our investigation, we consider a force surface that is required to be symmetric about the origin and has a total of nine unique control points. We consider the harmonic excitation to have fixed parameters, and sample SVs four times each excitation period, each sample taken after an evolution time of half a period. These conditions match those for the earlier optimization of the controller that has polynomial terms in Eq. (9).

Next, we present one case of these optimizations as an illustration of the effectiveness of the spline-surface feedback method. For a system having $b=0.1$ and $\omega_n=1$, a maximum force output of 3, and no attractor penalties between 1 and 5, the polynomial controller in Eq. (9) was optimized by adjusting the parameters (A,b_c,k_c,α_c) in increments of either 0.05 or 0.025 with possible initial values of A in the set $[0.1,0.5]$, b_c in the set $[0,1]$, and α_c in the set $[0,1]$ for 150 different initial cases. (The value of k_c was left un-initialized because it is always optimized first in our particular algorithm.) The parameter sets resulting in the highest magnitude SV are highlighted in Table 1.

When we consider the system under the same constraints but having its feedback of the form found in Eq. (10), we observe greater SV magnitudes. By initializing the spline surface over many different random initial surfaces that are symmetric about the $x-\dot{x}$ line and optimizing, we can arrive at a SV magnitude of 11.06 for the system shown in Figures 6 and 7, where the attractor is shown as the thickened black line superimposed over the spline surface.

This specific example is not an isolated case of higher sensitivity. When using spline force surfaces for state feedback,

TABLE 1. HIGH SENSITIVITY PARAMETER COMBINATIONS FOR POLYNOMIAL CONTROL

Set	k_c	α_c	A	b_c	SV Magnitude
1	-2.3	0.2	0.2	0	7.03
2	0	0	0.5	0	7.01
3	-1.3	0.05	0.4	0	6.95
4	0.35	-0.05	0.5	0	6.78
5	-2.1	0.15	0.2	0	6.61
6	-1.7	0.1	0.35	0	6.00

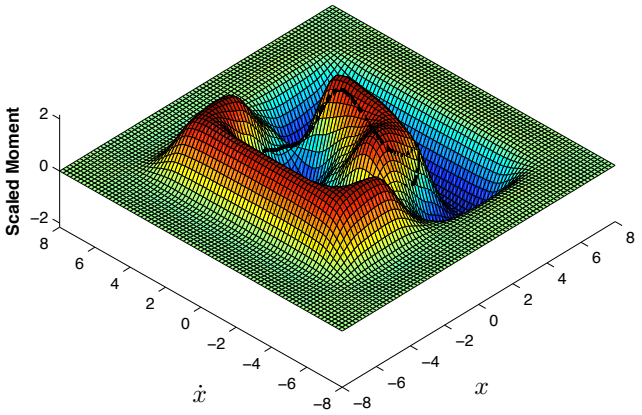

FIGURE 6. HIGH SENSITIVITY SPLINE FORCE SURFACE: ANGLED VIEW

almost all the initial parameter sets that we optimized resulted in higher sensitivities than in the case of a polynomial force controller. Part of this comparison is undoubtedly unfair since the polynomial controller has fewer adjustable parameters with which to begin. Nonetheless, it seems clear in examining the topology of the optimized spline force surfaces, that this type of feedback surface would be difficult to construct with a low number of polynomial terms. When the constraint on the symmetry of the force surface is removed, we can generate even higher sensitivities when all the other constraints are fixed. Table 2 shows the values of the three highest sensitivity regimes for a non-symmetric controller.

This is somewhat expected, since giving the optimizer more freedom in the parameter space should result in improved solutions, but it does highlight how significantly the assumed form of the controller function can effect its ability to provide the highest sensitivity regimes. We also attempted to optimize sensitivity using a larger number of control points to determine whether increasing the number of points could lead to large improvements in sensitivity. When the number of points was doubled for the case of the symmetric controller, this sometimes did not lead to significantly improved sensitivities; however, in the case of greatest improvement the sensitivity roughly doubled. Thus, we believe a more varied or "wavy" surface can sometimes yield significantly higher sensitivity regimes.

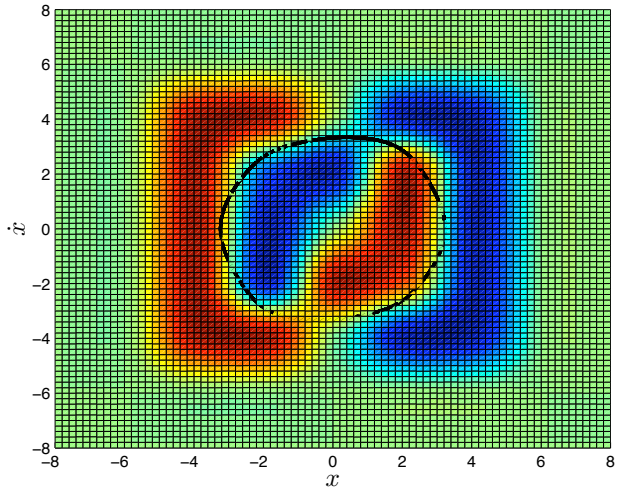

FIGURE 7. HIGH SENSITIVITY SPLINE FORCE SURFACE: TOP VIEW

TABLE 2. HIGH SENSITIVITY RESULTS FOR NON-SYMMETRIC SPLINE SURFACE

Set	Sensitivity Improvement Multiplier
1	17.31
2	15.71
3	15.32

APPLICATION TO FLUID SENSOR SYSTEMS

The techniques in the section above are directly applicable to fluid sensor systems once they have been reduced to 1 DOF, first-order state space systems as previously outlined. As a specific example, consider the inclined plate geometry and $x = \theta$. The suitably transformed system will have values of $b = 2.5 \cdot 10^4 \mathrm{s}^{-2}$

and $\omega_n = 6.4 \cdot 10^4 \text{s}^{-1}$. Bounding the spline surface between $\pm 1 \cdot 10^8 \text{s}^{-2}$ while considering several different combinations of A and ω allows for the calculation of various optimal controllers. Initial conditions for the spline surface were generated by dividing the total possible range by five and assigning a certain level of feedback for each of the nine control points in a specified pattern or at random. One example of a specific pattern has all of the inner points closest to the origin assigned one value (either positive or negative) and all of the outer points farther from the origin assigned another value (again, either positive or negative). The parameter of interest, to which we want to increase the sensitivity, can be either I or ω_n.

Results obtained while specifying ω_n as the parameter of interest have shown that, in some cases, the optimization can result in SV magnitudes improving several times over the initial, pseudo-random feedback surface. In the best cases, we were able to improve sensitivity tenfold. Almost all of the returned results are limit cycle attractors; this is expected based on our previous work. However, these limit cycles sometimes do not have the same period as the forcing harmonic due to the influence of the spline surface feedback.

A larger set of optimizations was also conducted for the same system with completely random initial conditions selected on an interval centered on zero. Various combinations of surface constraints and harmonic forcing magnitudes and frequencies were explored. One hundred trials were carried out for each specific combination. Depending on the case, the individual initial values were constrained to be between ten and fifty percent of the allowable range. We saw much more diversity in the resulting optimal attractors for this larger set of simulations, including some chaotic attractors. Again, we found that sensitivity could be improved over the base value by about ten times for cases which were already quite sensitive due to the forcing frequency approaching the natural frequency.

Even greater sensitivity improvements are possible when either the spline surface magnitude constraint is relaxed or a larger number of points are used to define the surface. When the allowable magnitude is doubled, and for a driving frequency of $\omega_d = 6.0 \cdot 10^4 \text{s}^{-1}$, Table 3 lists the three greatest improvements in sensitivity over the initial values.

Both chaotic and limit cycle cases are included in these attractors. Figures 8 and 9 show plots of two of the locally optimal surfaces and their attractors. If instead of increasing the allowable moment, the number of points used to define the surface is increased, sensitivity can also be greatly improved. In these cases, most of the high sensitivities are generated by chaotic attractors. Table 4 lists the three surfaces showing the greatest improvement in sensitivity over the initial conditions and Figure 10 shows one of these high sensitivity surfaces and its attractor.

If we instead consider the parallel plate geometry, the suitably transformed system will have values of $b = 3.9 \cdot 10^5 \text{s}^{-2}$ and $\omega_n = 9.8 \cdot 10^4 \text{s}^{-1}$. We bound the spline surface as before and then consider simulations, again choosing completely random initial conditions selected from an interval centered on zero and constrained to be between ten and fifty percent of the overall constraint range. We can again generate improvements in sensitivity that are several tens of times what was seen in the base case.

TABLE 3. SENSITIVITY IMPROVEMENTS DUE TO CHANGES TO SURFACE CONSTRAINTS

Set	Sensitivity Improvement Multiplier
1	21.7
2	11.6
3	11.3

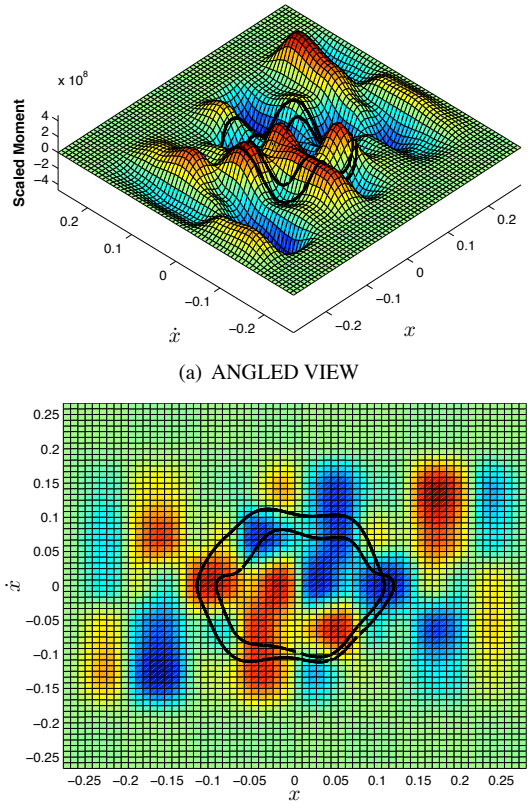

(a) ANGLED VIEW

(b) TOP VIEW

FIGURE 8. HIGH SENSITIVITY LIMIT CYCLE ATTRACTOR FOR THE ANGLED PLATE SENSOR

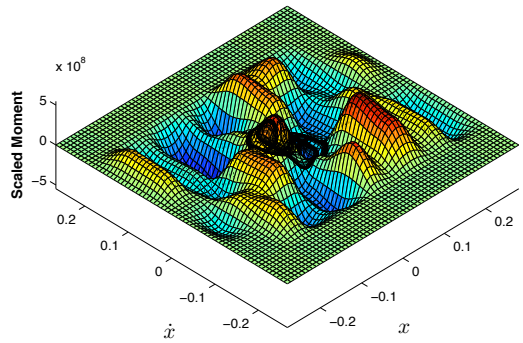

(a) ANGLED VIEW

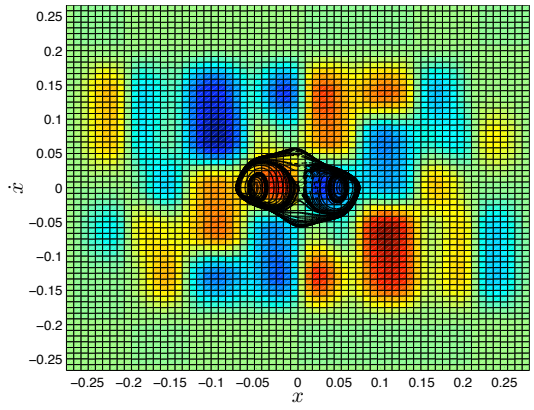

(b) TOP VIEW

FIGURE 9. HIGH SENSITIVITY CHAOTIC ATTRACTOR FOR THE ANGLED PLATE SENSOR

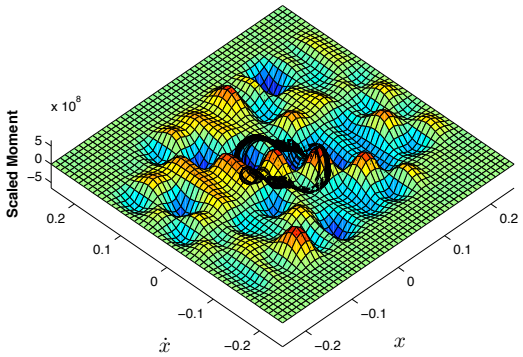

(a) ANGLED VIEW

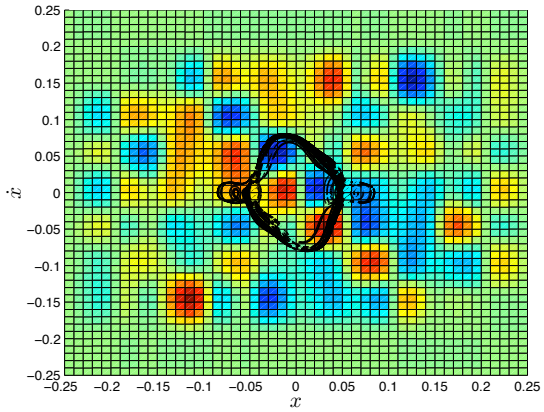

(b) TOP VIEW

FIGURE 10. HIGH SENSITIVITY CHAOTIC ATTRACTOR BASED ON A FINER SURFACE MESH

TABLE 4. SENSITIVITY IMPROVEMENTS DUE TO A HIGHER NUMBER OF INTERPOLATION POINTS

Set	Sensitivity Improvement Multiplier
1	28
2	24.8
3	19.4

CONCLUSIONS AND FUTURE WORK

We have demonstrated that for the low Reynolds number and high blockage ratio regimes involved in enclosed micro-system channel flow, it is difficult to design a geometry which will harvest energy from the oncoming flow and thereby reduce the effective damping ratio. Work involving a fluctuating incoming flow shows that we can generate motion in this case.

Using spline surfaces to define feedback forces over the state space and then optimizing these surfaces in order to maximize SV magnitude was shown to be an effective technique. We have illustrated how SVF techniques in conjunction with spline surfaces can be applied to our immersed sensors if they are modeled as simple 1 DOF systems. We have furthermore shown how this feedback can be optimized, leading to large improvements in sensitivity. Thus, we have shown SV techniques are effective in improving sensitivity, and may allow sensing in highly damped environments where traditional frequency-shift methods are not an alternative.

ACKNOWLEDGMENT

The authors would like to recognize the support of the National Science Foundation and the support of the Natural Sciences and Engineering Research Council of Canada through the PGS program.

REFERENCES

[1] Ilic, B., Craighead, H.G., Krylov, S., Senaratine, W., Ober, C., and Neuzil, P., 2004, "Attogram Detection Using Nanoelectromechanical Oscillators," *Journal of Applied Physics* **95**, pp. 3694-3703.

[2] Thundat, T., Wachter, E.A., Sharp, S.L., and Warmack, R.J., 1995, "Detection of Mercury-Vapor Using Resonating Micocantilevers," *Journal of Vacuum Science and Technology* **19**(6), pp. 2825-2828.

[3] Burg, T., Mirza, A., Milovic, N., Tsau, C., Popescu, G., Foster, J., and Manalis, S., 2006, "Vacuum-Packaged Suspended Micro-channel Resonant Mass Sensor for Biomolecular Detection," *Journal of Micro-Electro-Mechnical Systems* **15**(6), pp. 1466-1476.

[4] Judy, J., Maynes, D. and Webb, B.W., "Characterization of Frictional Pressure Drop for Liquid Flows Through Microchannels," *International Journal of Heat and Mass Transfer* **45**, pp. 3477-3489.

[5] Laser, D.J. and Santiago, J.G., 2004, "A Review of Micropumps," *Journal of Micromechanical Microengineering* **14**, pp. R35-R64.

[6] Robertson, I., Li L., Sherwin, S.J. and Bearman, P.W., 2003, "A Numerical Study of Rotational and Transverse Galloping Rectangular Bodies," *Journal of Fluids and Structures* **17**, pp. 681-699.

[7] Nakamura, Y. and Mizota, T., 1975, "Torsional Flutter of Rectangular Prisms," *Journal of Engineering Mechanics Division* **2**, pp. 125-142.

[8] Epureanu, B.I. and Hashmi, A., 2006, "Parameter Reconstruction Based on Sensitivity Vector Fields," *Journal of Vibration and Acoustics* **128**(6), pp. 732-740.

[9] Hashmi, A. and Epureanu, B.I., 2006, "Sensitivity Resonance and Attractor Morphing Quantified by Sensitivity Vector Fields for Parameter Reconstruction," *Nonlinear Dynamics* **45**(2), pp. 319-335.

[10] Yin, S.H. and Epureanu, B.I., 2007, "Experimental Enhanced Nonlinear Dynamics and Identification of Attractor Morphing Modes for Damage Detection," *Journal of Vibration and Acoustics* **129**(6), pp. 763-770.

[11] Yin, S.H. and Epureanu, B.I., 2006, "Nonlinear Feedback Excitation for System Interrogation by Bifurcation Morphing," *AIAA Journal* **46**(8), pp. 2058-2065.

[12] Yin, S.H. and Epureanu, B.I., 2005, "Enhanced Nonlinear Dynamics and Monitoring Bifurcations Morphing for the Identifcation of Parameter Variations," *Journal of Fluid and Structures* **21**(5-7), pp. 543-559.

[13] Lim, J. and Epureanu, B.I., 2010, "Sensitivity Vector Fields for Atomic Force Microscopes," *Nonlinear Dynamics* **59**, pp. 113-128.

[14] Sodano, H.A., Inman, D.J. and Park, G., 2004, "A Review of Power Harvesting from Vibration using Piezoelectric Materials," *The Shock and Vibration Digest* **36**, pp. 197-205.

[15] Anton, S.R. and Sodano, H.A., 2007, "A review of Power Harvesting using Piezoelectric Materials," *Smart Materials and Structures* **16**, pp. R1-R21.

[16] Naudascher, E. and Rockwell, D., 2000, Flow-Induced Vibrations: An Engineering Guide, A.A. Balkema, Rotterdam, Chap. 7-9.

[17] Blevins, R. D., 1990, Flow-Induced Vibration, Van Nostrand Reinhold, New York, NY, Chap 4.

[18] Newman, J.N., 1977, Marine Hydrodynamics, MIT Press, Cambridge, MA.

[19] Sloboda, A. R. and Epureanu, B.I., 2009, "Optimally Designed Nonlinear Feedback Excitation for High-Senisitivty Sensing," Proc. ASME 2009 SMASIS, Oxnard, CA.